

Adsorption and Corrosion Inhibition of *Atropa Belladonna* Extract on Carbon Steel in 1 M HCl Solution

K. Shalabi^{1,*}, Y.M. Abdallah², Hala M. Hassan³, A.S. Fouda¹

¹ Department of Chemistry, Faculty of Science, Mansoura University, Mansoura-35516, Egypt.

² Faculty of Oral and Dental medicine, Delta University for science and Technology, Gamasa, Egypt.

³ Textile Technology Department, Industrial Education College, Beni-Suef University, Egypt and Chemistry Department, Faculty of Science, Jazan University, KSA

*E-mail: dr_kemo84@yahoo.com

Received: 12 September 2013 / Accepted: 30 October 2013 / Published: 5 January 2014

The inhibition effect of *Atropa Belladonna* extract (ABE) on the corrosion of carbon steel in 1 M HCl solution was investigated by potentiodynamic polarization, electrochemical impedance spectroscopy (EIS) and electrochemical frequency modulation (EFM) techniques. The adsorption process obeyed a Langmuir adsorption isotherm. ABE acts as a mixed-type but mainly anodic inhibitor in 1 M HCl. The calculated adsorption thermodynamic parameters indicated that the adsorption was a spontaneous, exothermic process accompanied by an increase in entropy. The maximum inhibition approached 96.6% in the presence of 500 ppm ABE using Tafel polarization technique. Quantum chemical parameters were also calculated, which provided reasonable theoretical explanation for the adsorption and inhibition behavior of ABE on C-steel. ABE constituents have been simulated as adsorbate on Fe (1 1 0) substrate and the adsorption energy have been identified on iron surface. The results obtained from different electrochemical techniques and theoretical calculations were in good agreement.

Keywords: Carbon steel, Corrosion inhibition, *Atropa Belladonna*, HCl, Potentiodynamic polarization, EIS, EFM, Quantum calculation.

1. INTRODUCTION

The use of inhibitors is one of the most practical methods for protection against corrosion, especially in acidic media [1] where it is critical to prevent unexpected metal dissolution and acid consumption [2].

Most inhibitors used in industry are organic compounds primarily composed of nitrogen, oxygen and sulphur atoms. Inhibitors containing double or triple bonds play an important role in facilitating the adsorption of these compounds onto metal surfaces [3]. A bond can be formed between

the electron pair and/or the π -electron cloud of the donor atoms and the metal surface, thereby reducing corrosive attack in an acidic medium. Although many of these compounds have high inhibition efficiencies, several have undesirable side effects, even in very small concentrations, due to their toxicity to humans, deleterious environmental effects, and its high-cost [4].

Plant extract is low-cost and environmental safe, so the main advantages of using plant extracts as corrosion inhibitor are economic and safe environment. Up till now, many plant extracts have been used as effective corrosion inhibitors for iron or steel in acidic media, such as: *Matricaria recutita* [5], *Moringa oleifera* [6], henna [7], *Nypa fruticans* Wurmb [8], , olive [9], *Phyllanthus amarus* [10], *Occimum viridis* [11], lupine [12], *Vernonia amygdalina* [13], *Hibiscus rosa* [14], *Strychnos nux-vomica* [15], *Justicia gendarussa* [2], coffee [3], fruit peel [16] and Halfabar [17]. Besides steel, aluminum in acidic [18] and alkaline media [19], zinc in HCl solution [20], and Al–3Mg alloy in neutral NaCl solution [21] were protected against corrosion using some plant extracts. The inhibition performance of plant extract is normally ascribed to the presence of complex organic species, including tannins, alkaloids and nitrogen bases, carbohydrates and proteins as well as hydrolysis products in their composition. These organic compounds usually contain polar functions with nitrogen, sulfur, or oxygen atoms and have triple or conjugated double bonds or aromatic rings in their molecular structures, which are the major adsorption centers.

Atropa belladonna or *Atropabella-donna*, commonly known as Belladonna is a perennial herbaceous plant in the family Solanaceae, which native to Europe, North Africa, and Western Asia. Belladonna has been used in herbal medicine for centuries as a pain reliever, muscle relaxant, anti-inflammatory, also in treatment of menstrual problems, peptic ulcer disease, histaminic reaction, and motion sickness [22, 23].

The objective of this study was to investigate the inhibitory effect of *Atropa Belladonna* extract as a green corrosion inhibitor for carbon steel in 1 M hydrochloric acid using potentiodynamic polarization, electrochemical impedance spectroscopy, and electrochemical frequency modulation and quantum chemical calculations in detail.

2. EXPERIMENTAL

2.1. Materials and solutions

Experiments were performed using carbon steel of type 1018 with the following composition (weight %): C 0.2, Mn 0.6, P 0.04, Si 0.003 and balance Fe. The aggressive solution used was prepared by dilution of analytical reagent grade 37% HCl with bidistilled water. The stock solution (2000 ppm) of ABE was used to prepare the desired concentrations by dilution with bidistilled water. The concentration range of ABE used was 50-500 ppm.

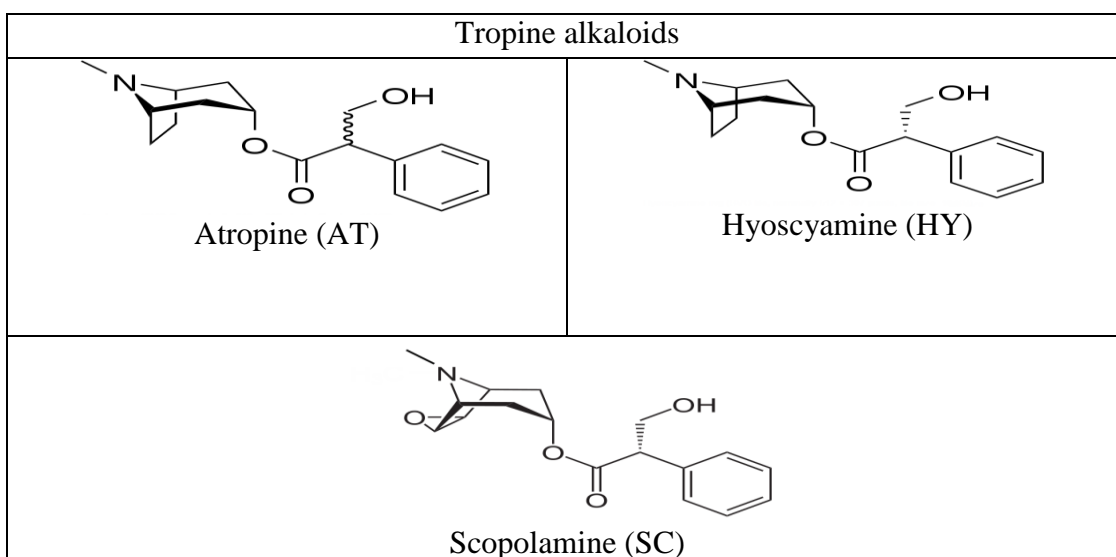
2.2. Preparation of plant extracts

Fresh aerial parts of *Atropa belladonna* were collected from Mansoura University garden, Mansoura, Egypt in spring (April 2013). Then identified by Botany Department, Faculty of Science,

Mansoura University. The sample was cut into small pieces, thoroughly washed with bidistilled water dried for a prolong period of time, grounded into powder and weighed (100 grams). Extraction of the stock solution was done by using reflux method. The plant material was extracted by soxhlet extractor using two different solvents of different polarities, petroleum ether at 60-80 °C to obtain petroleum ether fraction (fats and oils) followed by methanol to obtain methanol fraction which was evaporated and extracted with butanol to give butanol fraction which was again evaporated to give solid extract that was prepared for application as corrosion inhibitor.

Phytochemical analysis of *Atropa belladonna* reveals that the plant contains tropine alkaloids such as atropine (AT), hyoscyamine (HY) and scopolamine (SC) [24, 25].

Main constituents of *Atropa belladonna* extract are shown below:



2.3. Electrochemical measurements

Electrochemical measurements were performed using a typical three-compartment glass cell consisting of the carbon steel specimen as working electrode (1 cm²), saturated calomel electrode (SCE) as a reference electrode, and a platinum foil (1 cm²) as a counter electrode. The reference electrode was connected to a Luggin capillary and the tip of the Luggin capillary is made very close to the surface of the working electrode to minimize IR drop. All the measurements were done in solutions open to atmosphere under unstirred conditions. All potential values were reported versus SCE. Prior to each experiment, the electrode was abraded with successive different grades of emery paper, degreased with acetone, also washed with bidistilled water, and finally dried.

Tafel polarization curves were obtained by changing the electrode potential automatically from (-0.8 to 1 V vs. SCE) at open circuit potential with a scan rate of 1 mVs⁻¹. Stern-Geary method [26], used for the determination of corrosion current is performed by extrapolation of anodic and cathodic Tafel lines to a point which gives log i_{corr} and the corresponding corrosion potential (E_{corr}) for inhibitor free acid and for each concentration of inhibitor. Then i_{corr} was used for calculation of inhibition efficiency (η %) and surface coverage (θ) as in equation 1:

$$\eta \% = \theta \times 100 = [1 - (i_{\text{corr(inh)}} / i_{\text{corr(free)}})] \times 100 \quad (1)$$

where $i_{\text{corr(free)}}$ and $i_{\text{corr(inh)}}$ are the corrosion current densities in the absence and presence of inhibitor, respectively.

Impedance measurements were carried out in frequency range from 100 kHz to 0.1 Hz with amplitude of 5 mV peak-to-peak using ac signals at open circuit potential. The experimental impedance was analyzed and interpreted based on the equivalent circuit. The main parameters deduced from the analysis of Nyquist diagram are the charge transfer resistance R_{ct} (diameter of high-frequency loop) and the double layer capacity C_{dl} . The inhibition efficiencies and the surface coverage (θ) obtained from the impedance measurements are calculated from equation 2:

$$\eta \% = \theta \times 100 = [1 - (R_{\text{ct}}^{\circ} / R_{\text{ct}})] \times 100 \quad (2)$$

where R_{ct}° and R_{ct} are the charge transfer resistance in the absence and presence of inhibitor, respectively.

Electrochemical frequency modulation, EFM, was carried out using two frequencies 2 and 5 Hz. The base frequency was 0.1 Hz, so the waveform repeats after 1 s. The higher frequency must be at least two times the lower one. The higher frequency must also be sufficiently slow that the charging of the double layer does not contribute to the current response. Often, 10 Hz is a reasonable limit. The Intermodulation spectra contain current responses assigned for harmonical and intermodulation current peaks. The large peaks were used to calculate the corrosion current density (i_{corr}), the Tafel slopes (β_{a} and β_{c}) and the causality factors CF-2& CF-3 [27]. The electrode potential was allowed to stabilize 30 min before starting the measurements. All the experiments were conducted at $25 \pm 1^{\circ}\text{C}$.

All electrochemical measurements were performed using Gamry Instrument (PCI4/750) Potentiostat/Galvanostat/ZRA. This includes a Gamry framework system based on the ESA 400. Gamry applications include DC105 software for potentiodynamic polarization, EIS 300 software for electrochemical impedance spectroscopy, and EFM 140 software for electrochemical frequency modulation measurements via computer for collecting data. Echem Analyst 6.03 software was used for plotting, graphing, and fitting data.

To test the reliability and reproducibility of the measurements, duplicate experiments, which performed in each case at the same conditions.

2.4. Quantum chemical calculations

The correlation between theoretically calculated properties and experimentally determined inhibition efficiencies has been studied successfully for uniform corrosion [28]. Several theoretical parameters include the electronic properties of inhibitors, effect of the frontier molecular orbital energies, differences between lowest unoccupied molecular orbital (LUMO) and highest occupied molecular orbital (HOMO) energies ($E_{\text{LUMO}} - E_{\text{HOMO}}$), electronic charges on reactive centers, dipole moments and conformation of molecules investigated by semi-empirical methods (PM3) in Materials Studio 6.0 software from Accelrys Inc.

2.5. Molecular dynamics simulation

The molecular dynamics (MD) simulations as well as quantum chemical calculations were performed using the Materials Studio software [29]. The MD simulation of the interaction between tropane alkaloids and Fe (1 1 0) surface was carried out in a simulation box ($12.42\text{\AA}\times 12.42\text{\AA}\times 28.2\text{\AA}$) with periodic boundary conditions to model a representative part of the interface devoid of any arbitrary boundary effects. The Fe (1 1 0) surface was first built and relaxed by minimizing its energy using molecular mechanics, then the surface area of Ni (1 1 0) was increased and its periodicity was changed by constructing a super cell, and then a vacuum slab with 20\AA thicknesses was built on the Fe (1 1 0) surface. The number of layers in the structure was chosen so that the depth of the surface is greater than the non-bond cut off used in calculation. Using 6 layers of iron atoms gives a sufficient depth that the inhibitor molecules will only be involved in non-bond interactions with iron atoms in the layers of the surface, without increasing the calculation time. This structure then converted to have 3D periodicity. As 3D periodic boundary conditions are used, it is important that the size of the vacuum slab is great enough (20\AA) that the non-bond calculations for the adsorbate does not interact with the periodic image of the bottom layer of atoms in the surface.

After minimizing the Fe (1 1 0) surface and tropane alkaloid molecules, the corrosion system was built by layer builder to place the inhibitor molecules on Fe (1 1 0) surface, and the behavior of these molecules on the Fe (1 1 0) surface were simulated using the COMPASS (condensed phase optimized molecular potentials for atomistic simulation studies) force field. Adsorption locator module in Materials Studio 6.0 [29] has been used to model the adsorption of the inhibitor molecules onto Fe (1 1 0) surface and thus provide access to the energetic of the adsorption and its effects on the inhibition efficiencies of tropane alkaloids [30].

3. RESULTS AND DISCUSSION

3.1. Polarization curves

Figure 1 illustrates the polarization curves of carbon steel in 1 M HCl solution without and with various concentrations of ABE at 25°C . The presence of ABE shifts both anodic and cathodic branches to the lower values of corrosion current densities and thus causes a remarkable decrease in the corrosion rate. The parameters derived from the polarization curves in Figure 1 are given in Table 1. In 1 M HCl solution, the presence of ABE causes a remarkable decrease in the corrosion rate i.e., shifts both anodic and cathodic curves to lower current densities. In other words, both cathodic and anodic reactions of carbon steel electrode are retarded by ABE in hydrochloric acid solution. The Tafel slopes of β_a and β_c at 25°C do not change remarkably upon addition of ABE, which indicates that the presence of ABE does not change the mechanism of hydrogen evolution and the metal dissolution process. Generally, an inhibitor can be classified as cathodic or anodic type if the shift of corrosion potential in the presence of the inhibitor is more than 85 mV with respect to that in the absence of the inhibitor [31, 32]. In the presence of ABE, E_{corr} shifts to less negative but this shift is very small (about 20-30 mV),

which indicates that ABE can be arranged as a mixed-type inhibitor, with predominant anodic effectiveness.

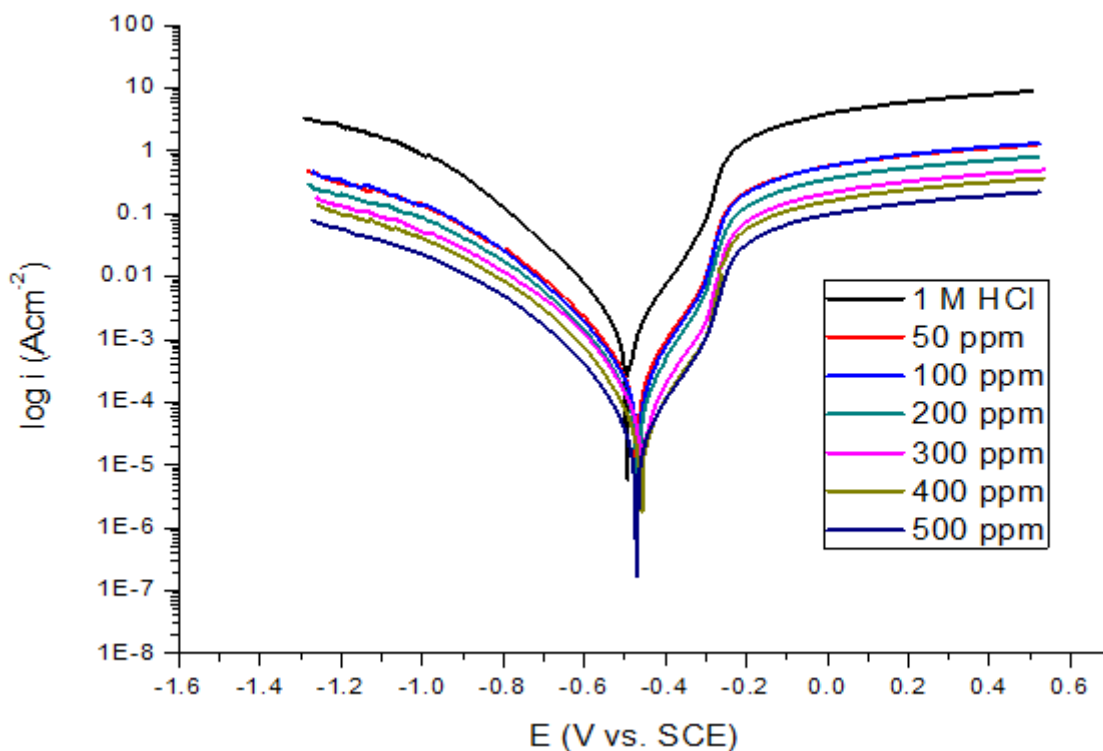


Figure 1. Potentiodynamic polarization curves for the corrosion of carbon steel in 1 M HCl solution without and with various concentrations of ABE at 25°C.

Table 1. Effect of concentration of ABE on the electrochemical parameters calculated using potentiodynamic polarization technique for the corrosion of carbon steel in 1 M HCl at 25°C.

Concentration, ppm	i_{corr} , $\mu\text{A cm}^{-2}$	$-E_{\text{corr}}$, mV vs. SCE	β_{a} , mVdec ⁻¹	β_{c} , mVdec ⁻¹	CR, mm y ⁻¹	\square	η %
1 M HCl	1260	493	110	161	574.6	--	--
50	364	471	131	189	166.1	0.711	71.1
100	276	468	117	180	125.9	0.781	78.1
200	185	468	119	185	84.4	0.853	85.3
300	128	456	149	188	58.6	0.898	89.8
400	87	459	174	189	28.3	0.931	93.1
500	55	471	151	188	24.9	0.956	95.6

3.2. Electrochemical impedance measurements (EIS)

Figures 2 and 3 show the Nyquist and Bode diagrams of carbon steel in 1 M HCl solutions containing different concentrations of ABE at 25°C. All the impedance spectra exhibit one single depressed semicircle.

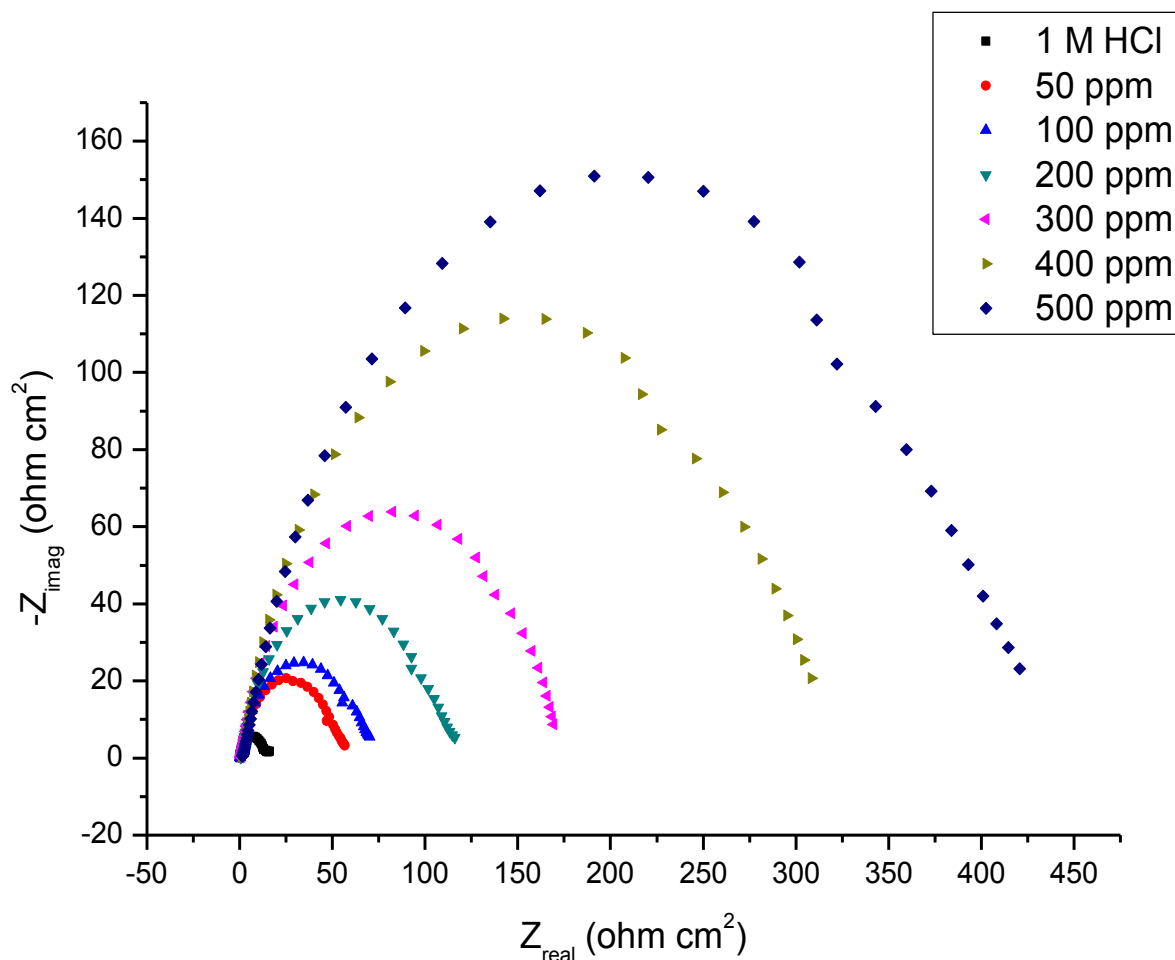


Figure 2. Nyquist plots recorded for carbon steel in 1 M HCl without and with various concentrations of ABE at 25°C.

The diameter of semicircle increases with the increase of ABE concentration. The impedance spectra exhibit one single capacitive loop, which indicates that the corrosion of steel is mainly controlled by a charge transfer process [33] and the presence of ABE does not change the mechanism of carbon steel dissolution [34]. In addition, these Nyquist diagrams are not perfect semicircles in 1 M HCl that can be attributed to the frequency dispersion effect as a result of the roughness and inhomogeneous of electrode surface [35]. Furthermore, the diameter of the capacitive loop in the presence of inhibitor is larger than that in the absence of inhibitor (blank solution), and increased with the inhibitor concentration. This indicates that the impedance of inhibited substrate increased with the inhibitor concentration. [34, 35]. This behavior is usually attributed to the inhomogeneity of the metal surface arising from surface roughness or interfacial phenomena [36], which is typical for solid metal electrodes [37]. Generally, when a non-ideal frequency response is presented, it is commonly accepted

to employ the distributed circuit elements in the equivalent circuits. What is most widely used is the constant phase element (CPE), which has a non-integer power dependence on the frequency [38]. Thus, the equivalent circuit depicted in Figure 4 is employed to analyze the impedance spectra, where R_s represents the solution resistance, R_{ct} denotes the charge-transfer resistance, and a CPE instead of a pure capacitor represents the interfacial capacitance. The impedance of a CPE is described by the equation 3:

$$Z_{CPE} = Y_0^{-1} (j\omega)^{-n} \tag{3}$$

where Y_0 is the magnitude of the CPE, j is an imaginary number, ω is the angular frequency at which the imaginary component of the impedance reaches its maximum values, and n is the deviation parameter of the CPE: $-1 \leq n \leq 1$. The values of the interfacial capacitance C_{dl} can be calculated from CPE parameter values Y_0 and n using equation 4 [39]:

$$C_{dl} = Y_0 (\omega_{max})^{n-1} \tag{4}$$

The values of the parameters such as R_s , R_{ct} , through EIS fitting as well as the derived parameters C_{dl} and η % are listed in Table 2.

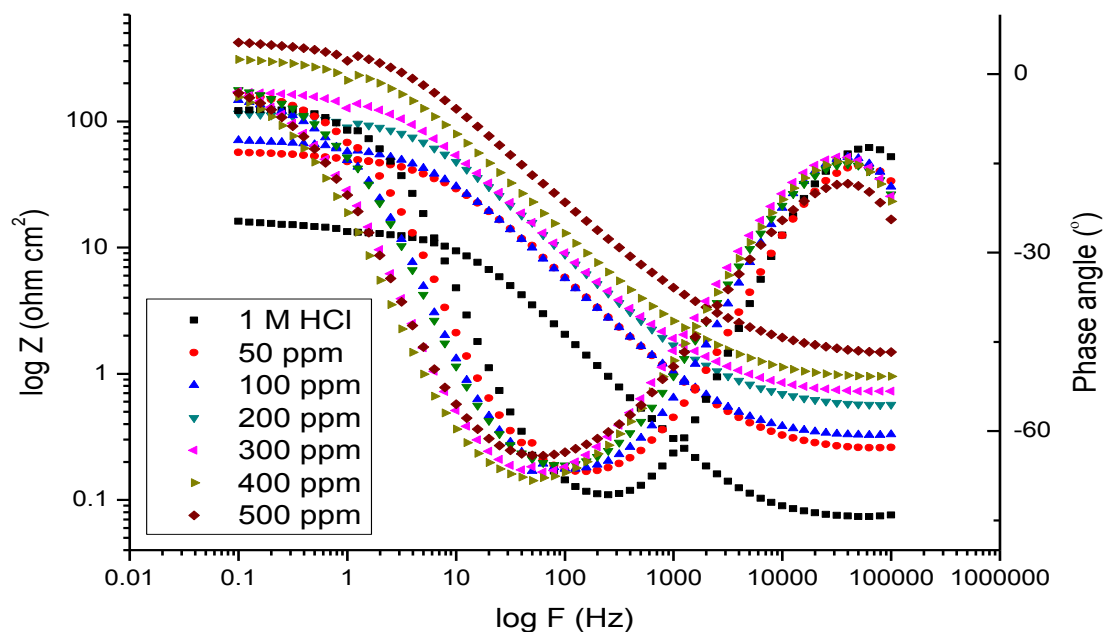


Figure 3. Bode plots recorded for carbon steel in 1 M HCl without and with various concentrations of ABE at 25°C.

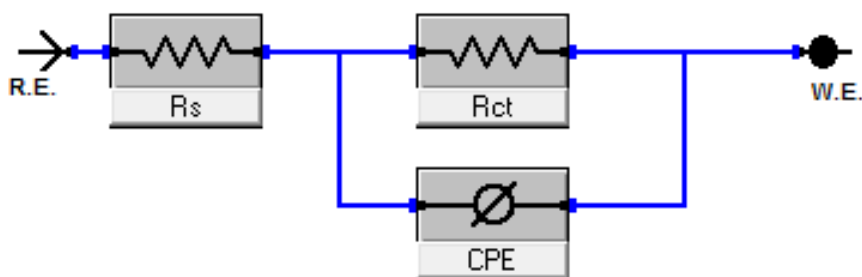


Figure 4. Electrical equivalent circuit used to fit the impedance data.

Table 2. Electrochemical kinetic parameters obtained from EIS technique for carbon steel in 1M HCl solution containing various concentrations of ABE at 25 °C.

Conc., ppm,	R_{ct} , $\Omega \text{ cm}^2$	C_{dl} , $\mu\text{F cm}^{-2}$	\square	$\eta \%$
1 M HCl	14.6	1066	--	--
50	55.6	450	0.738	73.8
100	69.0	433	0.789	78.9
200	113.5	332	0.871	87.1
300	174.0	327	0.916	91.6
400	312.0	263	0.953	95.3
500	430.9	165	0.966	96.6

3.3. Electrochemical frequency modulation measurements (EFM)

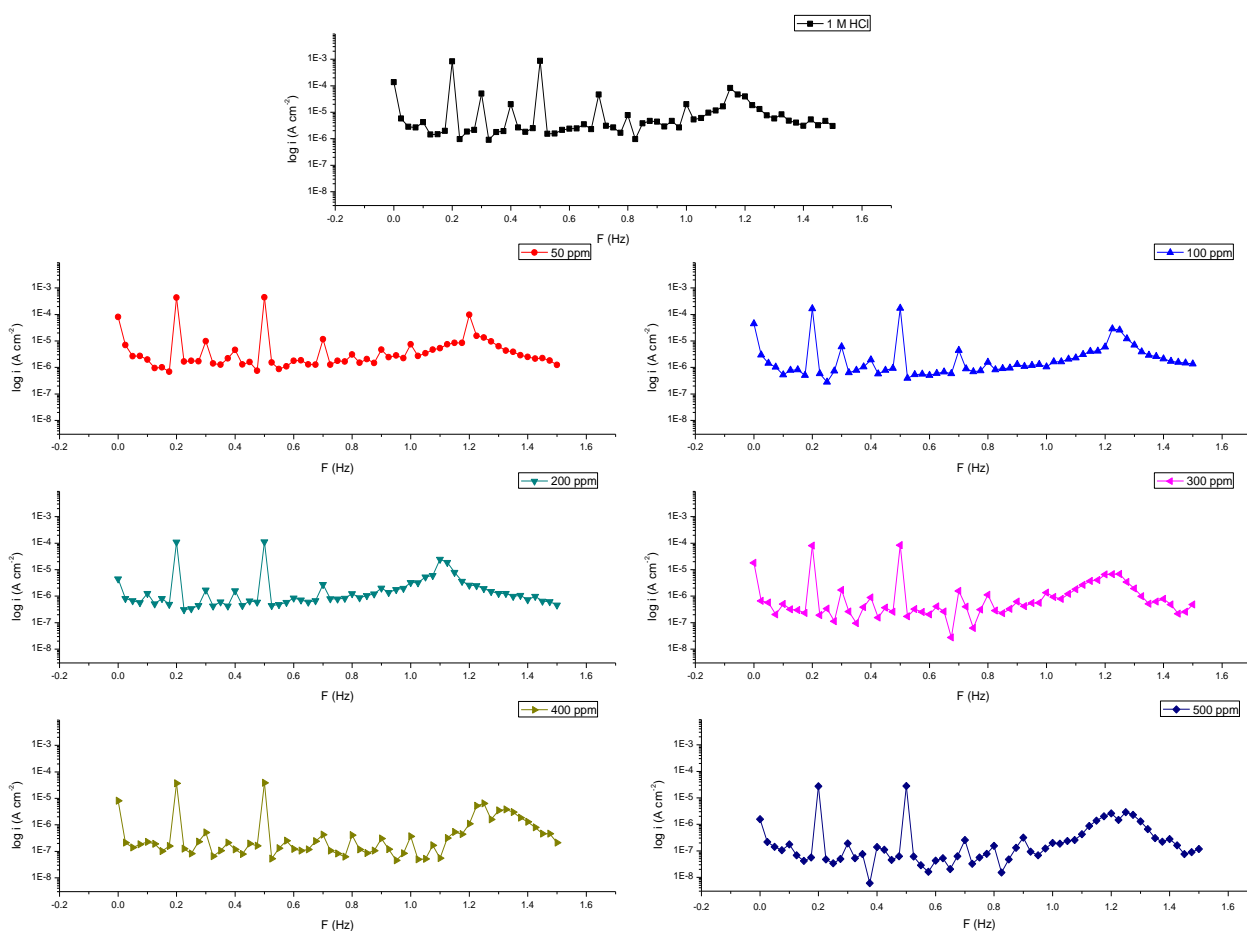


Figure 5 (a-g). Intermodulation spectrums for the corrosion of carbon steel in 1 M HCl without and with various concentrations of ABE at 25°C.

The EFM is a nondestructive corrosion measurement technique that can directly give values of the corrosion current without prior knowledge of Tafel constants. Like EIS, it is a small AC signal. Intermodulation spectra obtained from EFM measurements of carbon steel in 1 M HCl solution, in the absence and presence of different concentrations of the investigated extract at 25°C and 45°C, are presented in Figure 5a-g and Figure 6a-g. Each spectrum is a current response as a function of frequency.

The calculated corrosion kinetic parameters at different concentrations of the ABE in 1 M HCl at 25°C and 45°C (i_{corr} , β_a , β_c , CF-2, CF-3 and $\eta\%$) are given in Table 3. From this Table, the corrosion current densities decreased by increasing the concentration of investigated extract, the inhibition efficiencies increase by increasing investigated extract concentrations and decreases by increasing in temperature. The causality factors CF-2 and CF-3 in Table 3 are very close to theoretical values that according to EFM theory [41] should guarantee the validity of Tafel slopes and corrosion current densities.

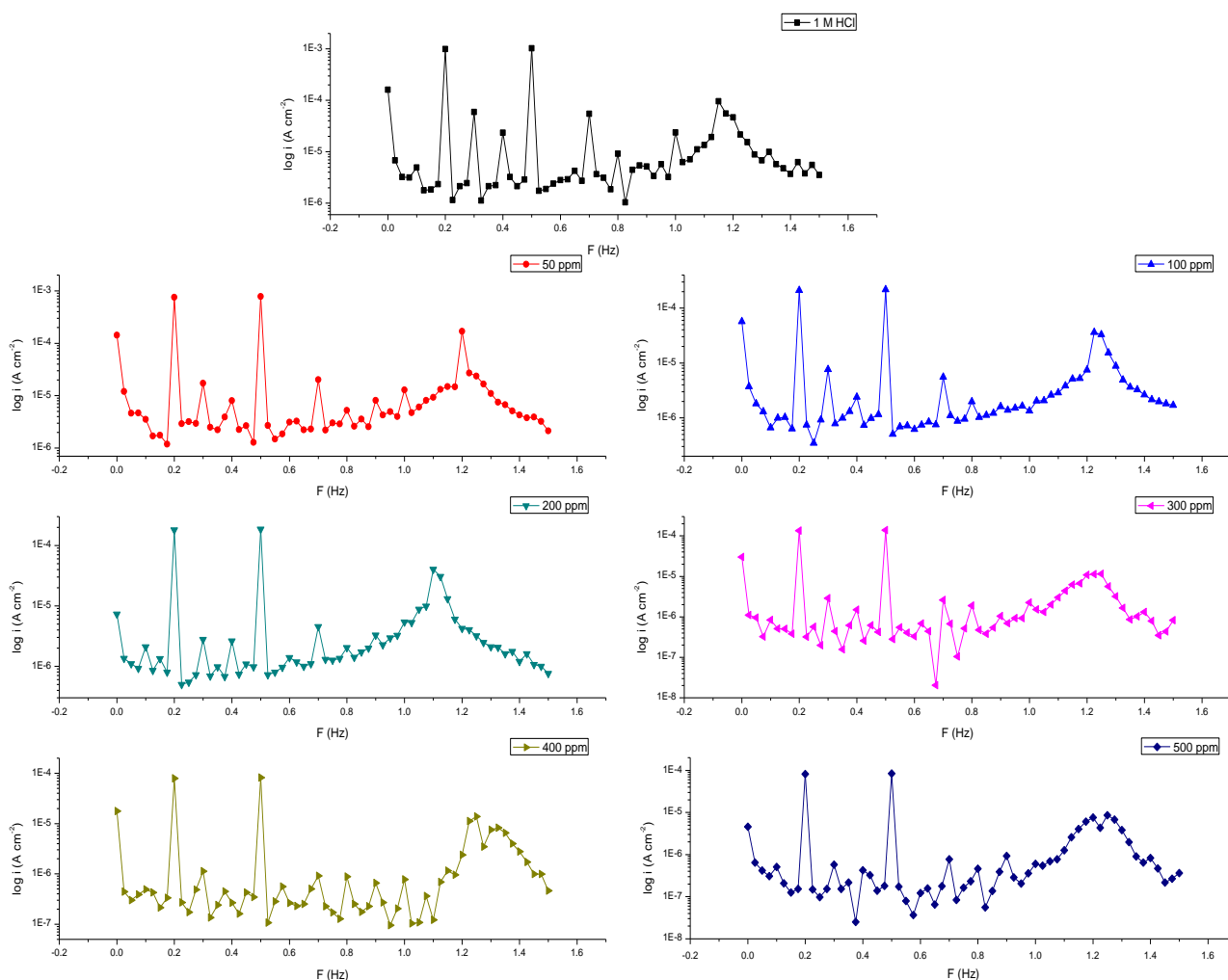


Figure 6 (a-g). Intermodulation spectrums for the corrosion of carbon steel in 1 M HCl without and with various concentrations of ABE at 45°C.

Values of causality factors in Table 3 indicates that the measured data are of good quality. The standard values for CF-2 and CF-3 are 2.0 and 3.0, respectively. The deviation of causality factors from their ideal values might due to that the perturbation amplitude was too small or that the resolution of the frequency spectrum is not high enough. Another possible explanation is that the inhibitor is not performing very well.

The results showed good agreement of corrosion kinetic parameters obtained from EFM with those obtained from Tafel extrapolation and EIS methods.

Table 3. Electrochemical kinetic parameters obtained by EFM technique for carbon steel in 1M HCl solution containing different concentrations of ABE at 25°C and 45°C.

Temp., °C	Conc., ppm	i_{corr} , $\mu\text{A cm}^{-2}$	β_a , mVdec^{-1}	β_c , mVdec^{-1}	CR, mm y^{-1}	CF-2	CF-3	\square	% η
25	1 M HCl	1231	81	112	562.0	2.29	2.95	--	--
	50	314	45	49	143.4	1.78	2.86	0.745	74.5
	100	258	91	110	117.9	2.12	2.82	0.790	79.0
	200	157	87	97	71.8	1.91	2.72	0.872	87.2
	300	89	68	74	40.7	1.85	3.35	0.928	92.8
	400	57	95	103	26.0	1.95	3.07	0.954	95.4
	500	29	67	69	13.2	1.92	3.00	0.976	97.6
45	1 M HCl	1452	80	113	663.2	2.43	3.18	--	--
	50	550	45	48	251.1	1.78	2.72	0.621	62.1
	100	326	90	110	148.8	2.30	2.53	0.776	77.6
	200	258	86	97	117.9	1.91	2.71	0.822	82.2
	300	149	67	74	67.9	2.42	2.72	0.898	89.8
	400	123	95	102	56.1	1.94	3.04	0.915	91.5
	500	86	66	69	39.3	2.32	2.86	0.941	94.1

3.4. Adsorption isotherm

It is generally assumed that the adsorption of the inhibitors on the metal surface is essential step in the inhibition mechanism [42]. To calculate the surface coverage θ it was assumed that the inhibitor efficiency is due mainly to the blocking effect of the adsorbed species and hence $\eta \% = 100 \times \theta$ [43]. In order to gain insight into the mode of adsorption of the extract on carbon steel surface, the surface coverage values from EFM technique were theoretically fitted into different adsorption isotherms and

the values of correlation coefficient (R^2) were used to determine the best-fit isotherm. Figure 7 shows the plot C/θ vs. C , which is typical of Langmuir adsorption isotherm at 25°C, and 45°C. Perfectly linear plot was obtained with regression constant (R^2) exceeding 0.9987 at 25°C and 0.9989 at 45°C and slope about unity. The deviation of the slope from unity, as observed from this study, could be interpreted to mean that there are interaction between adsorbate species on the metal surface as well as changes in adsorption heat with increasing surface coverage [44, 45], factors that were ignored in the derivation of Langmuir isotherm.

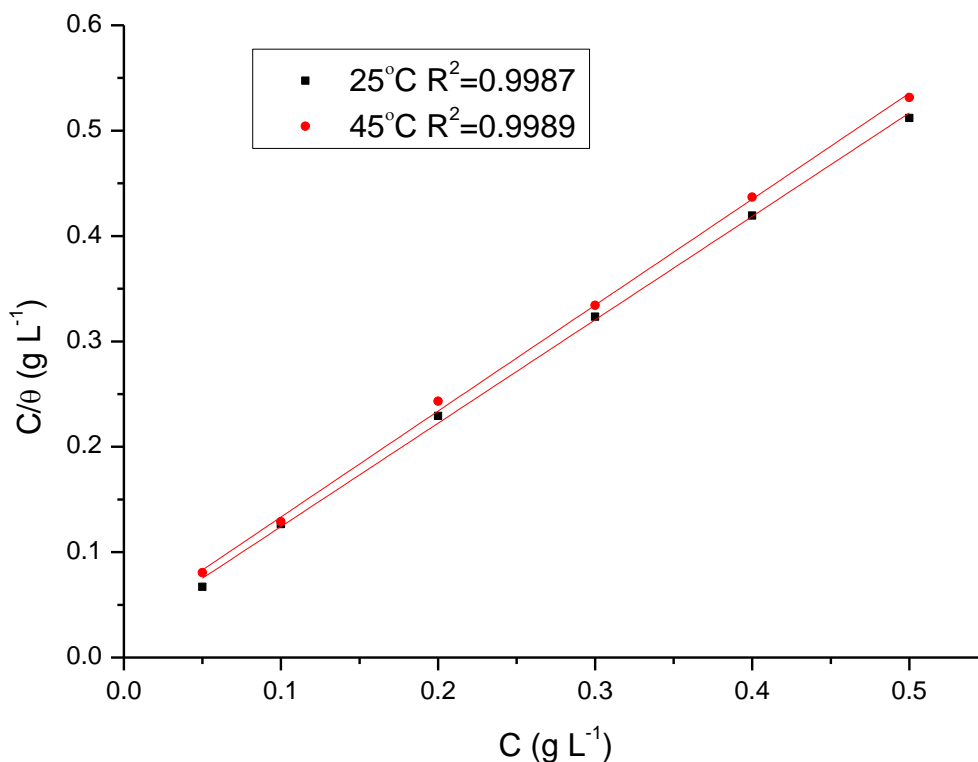


Figure 7. Curve fitting of corrosion data for carbon steel in 1 M HCl in the presence of different concentrations of ABE to Langmuir adsorption isotherm at 25°C & 45°C.

The Langmuir isotherm is given by equation 5 [46]:

$$C/\theta = 1/K + C \tag{5}$$

where C is the inhibitor concentration and K is the equilibrium constant of adsorption process and is related to the standard free energy of adsorption $\Delta G^\circ_{\text{ads}}$ by equation 6:

$$K = 1/55.5 \exp(-\Delta G^\circ_{\text{ads}}/RT) \tag{6}$$

The value of 55.5 is the concentration of water in solution expressed in mole per liter, R the universal gas constant and T the absolute temperature. The calculated $\Delta G^\circ_{\text{ads}}$ values were also given in Table 4. The negative values of $\Delta G^\circ_{\text{ads}}$ ensure the spontaneity of the adsorption process and the stability of the adsorbed layer on the carbon steel surface [47]. It is well known that values of $\Delta G^\circ_{\text{ads}}$ of the order of -40 kJ mol^{-1} or higher involve charge sharing or transfer from the inhibitor molecules to metal surface to form coordinate type of bond (chemisorption); those of order of -20 kJ mol^{-1} or lower

indicate a physisorption [48, 49]. The calculated $\Delta G^{\circ}_{\text{ads}}$ values (Table 4) were less negative than -20 kJmol^{-1} indicate, therefore, that the adsorption mechanism of the investigated extract on carbon steel in 1 M HCl solution is typical of physisorption. The lower negative values of $\Delta G^{\circ}_{\text{ads}}$ indicate that this inhibitor is not strongly adsorbed on the carbon steel surface. Moreover, $\Delta G^{\circ}_{\text{ads}}$ of the investigated extract is approximately constant for carbon steel.

Moreover, the adsorption heat can be calculated according to the Van't Hoff equation 7 [50]:

$$\ln K = -\frac{\Delta H^{\circ}_{\text{ads}}}{RT} + \text{const} \quad (7)$$

That is:

$$\ln\left(\frac{K_2}{K_1}\right) = -\frac{\Delta H^{\circ}_{\text{ads}}}{RT} \left(\frac{1}{T_2} - \frac{1}{T_1}\right) \quad (8)$$

where $\Delta H^{\circ}_{\text{ads}}$ is the adsorption heat, K_1 and K_2 are the adsorptive equilibrium constants at T_1 (25°C) and T_2 (45°C), respectively. In consideration that the experiments precede at the standard pressure and the solution concentrations are not very high, which are close to the standard condition, the calculated adsorption heat thus can be approximately regarded as the standard adsorption heat $\Delta H^{\circ}_{\text{ads}}$ [50]. The negative values of $\Delta H^{\circ}_{\text{ads}}$ (Table 4) reflect the exothermic behavior of the adsorption of ABE on the carbon steel surface.

Table 4. Equilibrium constant (K_{ads}) and adsorption free energy ($\Delta G^{\circ}_{\text{ads}}$) of ABE adsorbed on carbon steel surface in 1 M HCl at 25°C and 45°C .

Temp., $^{\circ}\text{C}$	Langmuir adsorption isotherm			
	$K_{\text{ads}} \times 10^{-5}$, g^{-1}	$-\Delta G^{\circ}_{\text{ads}}$, kJ mol^{-1}	$-\Delta H^{\circ}_{\text{ads}}$, kJ mol^{-1}	$\Delta S^{\circ}_{\text{ads}}$, $\text{J K}^{-1} \text{mol}^{-1}$
25	38.31	18.99	90.37	33.39
45	30.46	18.42	90.37	29.50

Finally, the standard adsorption entropy $\Delta S^{\circ}_{\text{ads}}$ can be calculated by the equation 9:

$$\Delta S^{\circ}_{\text{ads}} = \frac{\Delta H^{\circ}_{\text{ads}} - \Delta G^{\circ}_{\text{ads}}}{T} \quad (9)$$

The $\Delta S^{\circ}_{\text{ads}}$ values (Table 4) are positive, which are opposite to the usual expectation that the adsorption is an exothermic process and always accompanied by a decrease of entropy. The reason can be explained as follows: the adsorption of organic inhibitor molecules from the aqueous solution can be regarded as a quasi-substitution process between the organic compound in the aqueous phase [Org(sol)] and water molecules at the electrode surface [$\text{H}_2\text{O}(\text{ads})$] [51]. In this situation, the adsorption of ABE is accompanied by the desorption of water molecules from the electrode surface. Thus, while the adsorption process for the inhibitor is believed to be exothermic and associated

with a decrease in entropy of the solute, the opposite is true for the solvent [52]. The thermodynamic values obtained are the algebraic sum of the adsorption of organic inhibitor molecules and the desorption of water molecules [53]. Therefore, the gain in entropy is attributed to the increase in solvent entropy [52]. The positive values of $\Delta S_{\text{ads}}^{\circ}$ suggest that the adsorption process is accompanied by an increase in entropy, which is the driving force for the adsorption of ABE on the carbon steel surface. Table 4 lists all the above calculated thermodynamic parameters.

3.5. Quantum chemical calculation results

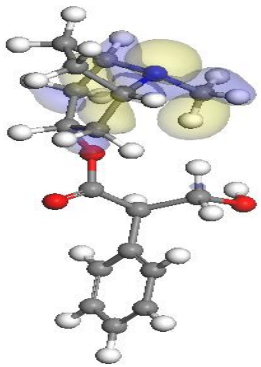
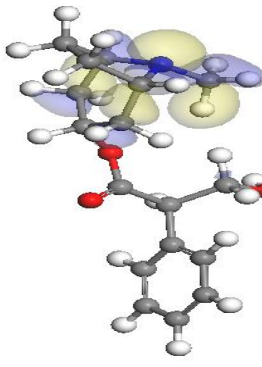
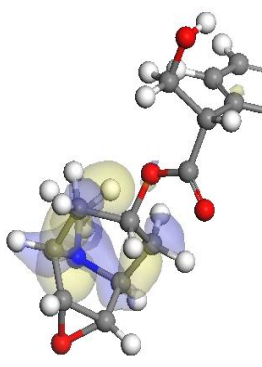
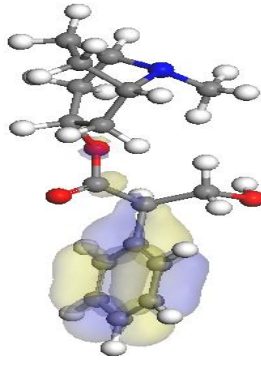
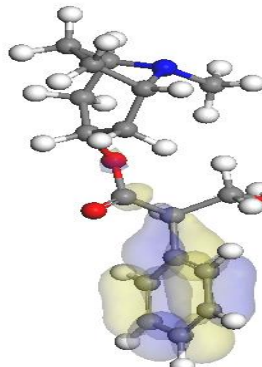
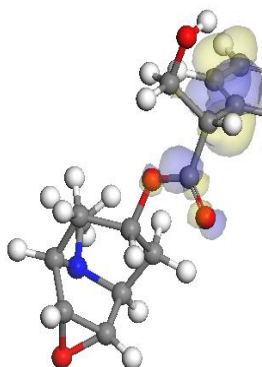
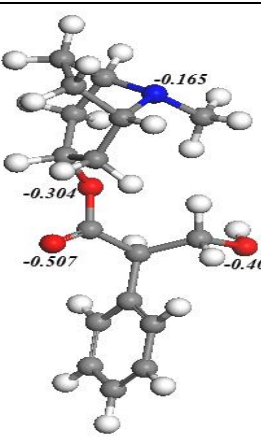
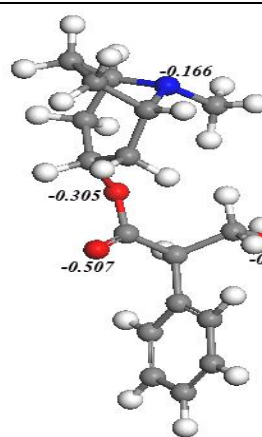
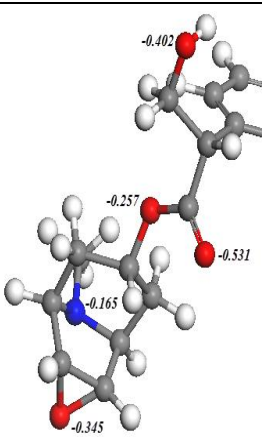
	Atropine	Hyoscyamine	Scopolamine
HOMO			
LUMO			
Mulliken atomic charges			

Figure 8. The optimized molecular structures, HOMO, LUMO and Mulliken atomic charges of the major effective molecules of ABE using PM3.

As known, the plant extract is a complex mixture of various phytochemical components. Atropine, hyoscyamine and scopolamine have been identified as the major chemical constituents of the plant extract. Hence, the quantum chemical calculations are performed to model the adsorption structures of these chemical constituents (hyoscyamine, scopolamine and atropine) in order to provide some insights into the nature of their interaction with the C-steel and their possible contributions to the overall inhibiting effect. Figure 8 illustrates the optimized structure, the lowest unoccupied molecular orbital (LUMO), and the highest occupied molecular orbital (HOMO) of atropine, hyoscyamine and scopolamine. It could be seen that the HOMO orbitals for AT, HY and SC are located on the tropane ring while the LUMO orbitals are located on the benzene ring. Figure 8 presents the Mulliken charge distributions of the studied molecules. The Mulliken population analysis is usually utilized for the calculation of the charge distribution over the whole skeleton of the molecule and thus help to estimate the adsorption centers of inhibitors [54, 55]. A general consensus of the Mulliken charge distributions is that the more negatively charged heteroatom the better action for the electron donor [56]. Table 5 lists some quantum chemical parameters, which are thought important due to their direct influence on electronic interaction between the inhibitor molecules and C-steel surface. E_{HOMO} , the energy of the highest occupied molecular orbital; E_{LUMO} , the energy of the lowest unoccupied molecular orbital; ΔE , the energy of $E_{\text{LUMO}} - E_{\text{HOMO}}$ and μ , the dipole moment. According to the frontier molecular orbital (FMO) theory [57], the electron transition is due to an interaction between the frontier orbitals (HOMO) and (LUMO) of the reacting species. E_{HOMO} levels are often associated with the electron donating ability of a molecule and the higher values of E_{HOMO} usually indicate a tendency of the molecule to donate electrons to the appropriate acceptor molecules with low energy and empty electron orbital. The value of E_{LUMO} is related to the ability of the molecule to accept electrons and the lower values of E_{LUMO} often mean that the inhibitor molecule likely accepts electrons. Consequently, the value of ΔE provides a measure for the stability of the formed complex on the metal surface. The lower values of ΔE reflect the higher stability of the formed complex [58, 59]. The dipole moment μ is a measure of the polarity of a covalent bond, which is related to the distribution of electrons in a molecule [60].

Although literature is inconsistent with the use of μ as a predictor for the direction of a corrosion inhibition reaction, it is generally agreed that the large values of μ favour the adsorption of inhibitor [60].

As is seen from Table 5, there are only small differences (less than 0.45 eV) between the values of E_{HOMO} for the different molecules, which indicate that these molecules have very similar capacities of charge donation to the metallic surface [61] and also they have similar values of E_{HOMO} and ΔE which implies the high ability to accept electrons from the d-orbital of Fe and the high stability of the [Fe–inh] complexes [7]. Moreover, SC has a rather high value of μ , which implies the strong adsorption of SC molecule at the C-steel surface and it has high molecular surface area which indicates that planar structure of SC molecule. Figure 8 covers the largest area of C-steel surface.

Table 5. The calculated quantum chemical parameters for the major effective components of ABE.

Parameter	Atropine	Hyoscyamine	Scopolamine
E_{HOMO} (eV)	-9.590	-9.601	-9.780
E_{LUMO} (eV)	-0.115	-0.116	-0.179
ΔE (eV)	9.475	9.451	9.601
μ (debyes)	2.483	2.451	3.633
Molecular area (\AA^2)	332.276	332.456	336.898

3.6. Molecular dynamics simulation

Figure 9 shows the most suitable configuration for adsorption of tropane alkaloids on Fe (1 1 0) substrate obtained by adsorption locator module [62] in Materials studio [63].

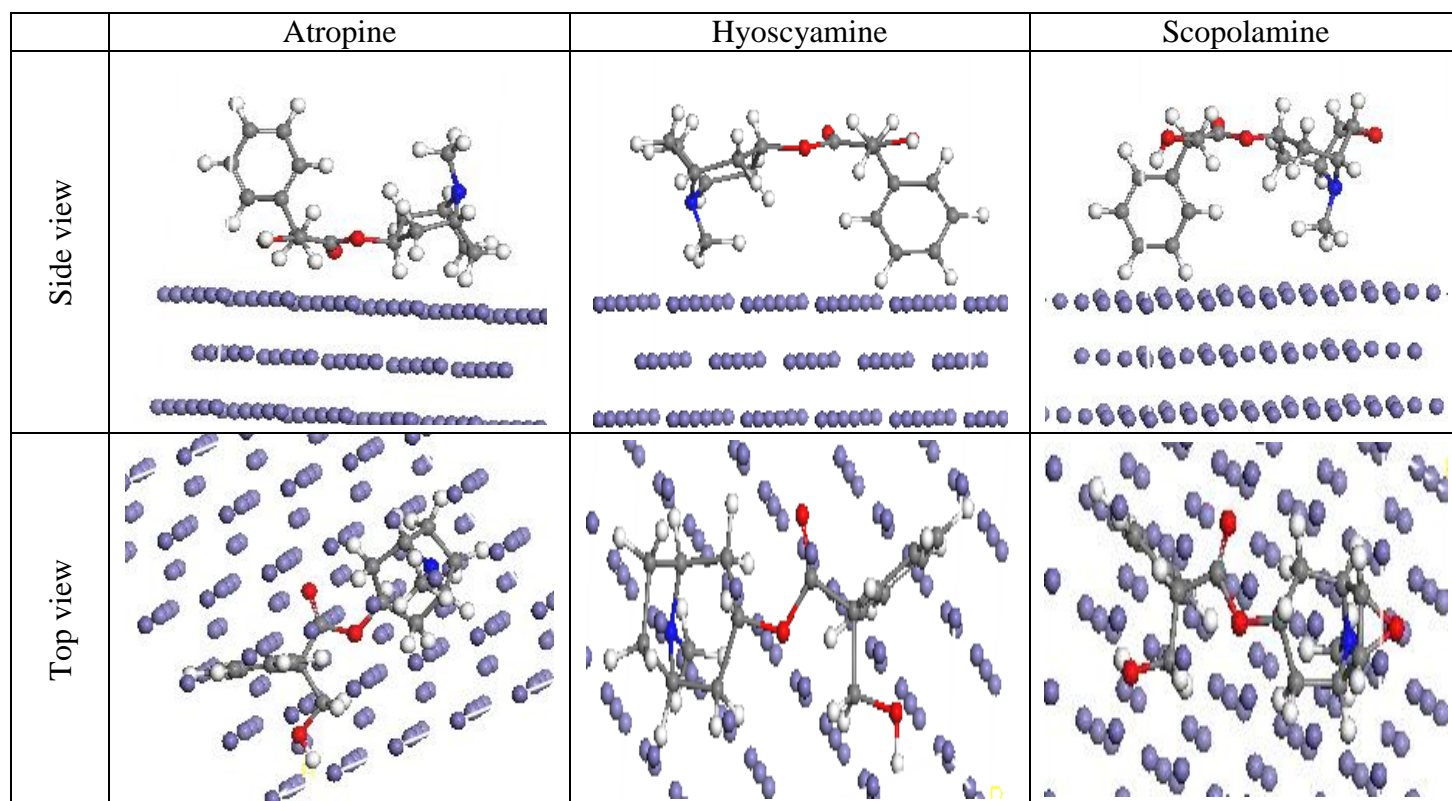


Figure 9. Most suitable configuration for adsorption of the major effective molecules of ABE on Fe (1 1 0) substrate obtained by adsorption locator module.

The outputs and descriptors calculated by the Monte Carlo simulation are presented in Table 6. The parameters presented in Table 6 includes total energy, in kcal mol^{-1} , of the substrate–adsorbate configuration. The total energy is defined as the sum of the energies of the adsorbate components, the rigid adsorption energy and the deformation energy. In this study, the substrate energy (iron surface) is

taken as zero. The adsorption energy in kcal mol^{-1} , reports energy released (or required) when the relaxed adsorbate components (tropane alkaloids) are adsorbed on the substrate surface. The adsorption energy is defined as the sum of the rigid adsorption energy and the deformation energy for the adsorbate components. The rigid adsorption energy reports the energy, in kcal mol^{-1} , released (or required) when the unrelaxed adsorbate components (i.e., before the geometry optimization step) are adsorbed on the substrate. The deformation energy reports the energy, in kcal mol^{-1} , released when the adsorbed adsorbate components are relaxed on the substrate surface. Table 6 shows also (dE_{ads}/dN_i), which reports the energy, in kcal mol^{-1} , of substrate-adsorbate configurations where one of the adsorbate components has been removed. As can be seen from Table 6, SC gives the maximum adsorption energy found during the simulation process. High values of adsorption energy indicate that SC is the most efficient inhibitor. Therefore, the studied molecules are likely to adsorb on the iron surface to form stable ad layers and protect iron from corrosion.

Table 6. Outputs and descriptors calculated by the Mont Carlo simulation for adsorption of tropane alkaloids on iron (1 1 0).

Inhibitor	Total energy (kcal mol^{-1})	Adsorption energy (kcal mol^{-1})	Rigid adsorption energy (kcal mol^{-1})	Deformation energy (kcal mol^{-1})	dE_{ads}/dN_i (kcal mol^{-1})
Atropine	-214.57	-153.81	-165.02	11.21	-153.81
Hyoscyamine	-214.87	-154.12	-165.10	10.98	-154.12
Scopolamine	-67.18	-152.83	-157.93	5.10	-152.83

3.7. Mechanism of inhibition

Most organic inhibitors contain at least one polar group with an atom of nitrogen or sulphur or in some cases selenium and phosphorus. The inhibiting properties of many compounds are determined by the electron density at the reaction center [64].

With increase in electron density in the center, the chemisorption between the inhibitor and the metal are strengthened [65, 66]. The plant extract ABE is composed of numerous naturally occurring organic compounds. Accordingly, the inhibitive action of ABE could be attributed to the adsorption of its components on the carbon steel surface. The main constituents of ABE are phytochemical constituents is tropane alkaloids [such as tropine, hyoscyamine and scopolamine). Most of these phytochemicals are organic compounds that have center for π -electron and presence of hetero atoms such as oxygen and nitrogen; hence, the adsorption of the inhibitor on the surface on carbon steel is enhanced by their presence. [67] reported that tropane alkaloids are major constituents of plants that enhance the inhibition potentials of plant extracts. Therefore, the inhibition efficiency of methanol extracts of ABE is due to the formation of multi-molecular layer of adsorption between iron in the carbon steel and some of these phytochemicals. Results of the present study have shown that ABE

extract inhibits the acid induced corrosion of carbon steel by virtue of adsorption of its components onto the metal surface. The inhibition process is a function of the metal, inhibitor concentration, and temperature as well as inhibitor adsorption abilities, which is so much dependent on the number of adsorption sites. The mode of adsorption (physiosorption) observed could be attributed to the fact that ABE contains many different chemical compounds, which some can be adsorbed physically. This observation may derive the fact that adsorbed organic molecules can influence the behaviour of electrochemical reactions involved in corrosion processes in several ways. The action of organic inhibitors depends on the type of interactions between the substance and the metallic surface. The interactions can bring about a change either in electrochemical mechanism or in the surface available for the processes [48, 68].

4. CONCLUSIONS

From the overall experimental results the following conclusions can be deduced:

1. ABE is good inhibitor and act as mixed type but mainly act as anodic inhibitors for carbon steel corrosion in 1 M HCl solution.
2. The results obtained from all electrochemical measurements showed that the inhibiting action increases with the inhibitor concentration and decreases with the increasing in temperature.
3. Double layer capacitances decrease with respect to blank solution when the plant extract is added. This fact confirms the adsorption of plant extract molecules on the carbon steel surface.
4. The adsorption of inhibitor on carbon steel surface in HCl solution follows Langmuir isotherm for ABE.
5. The values of inhibition efficiencies obtained from the different independent quantitative techniques used show the validity of the results.
6. Quantum chemical parameters and molecular dynamics simulation for ABE were calculated to provide further insight into the mechanism of inhibition of the corrosion process.

References

1. G.Trabanelli, *Corrosion*,47 (1991) 410.
2. A.K. Satapathy, G. Gunasekaran, S.C.Sahoo, K.Amit, R.V.Rodrigues, *Corros. Sci.*,51 (2009)2848.
3. V.V. Torres, R.S. Amado, C.F. de Sa, T.L. Fernandez, C.A.S. Riehl, A.G. Torres, E. D'Elia, *Corros. Sci.*, 53(2011) 2385.
4. D. Gopi, K.M. Govindaraju, L. Kavitha, *J.Appl. Electrochem.* 40 (2010) 1349.
5. M. Nasibi, D. Zaarei, G. Rashed, E. Ghasemi, *Chem. Eng. Comm.*200 (2013) 367.
6. A. Singh, I. Ahamad, D.K. Yadav, V.K. Singh, M.A. Quraishi, *Chem. Eng. Comm.*, 199 (2012) 63.
7. A. Ostovari, S.M. Hoseinie, M. Peikari, S.R. Shadizadeh, S.J. Hashemi, *Corros. Sci.*, 51 (2009) 1935.
8. K.O. Orubite, N.C. Oforika, *Mater. Lett.* 58 (2004) 1768.
9. A.Y. El-Etre, *J. Colloid Interface Sci.*314 (2007) 578.

10. P.C. Okafor, M.E. Ikpi, I.E. Uwah, E.E. Ebenso, U. J. Ekpe, S.A. Umoren, *Corros. Sci.* 50 (2008) 2310.
11. E.E. Oguzie, *Corros. Sci.* 50 (2008) 2993.
12. A.M. Abdel-Gaber, B.A. Abd-El-Nabey, M. Saadawy, *Corros. Sci.* 51 (2009) 1038.
13. N.O. Eddy, S.A. Odoemelam, A.O. Odiongenyi, *Portugaliae Electrochim. Acta.* 27 (2009) 33.
14. K. Anuradha, R. Vimala, B. Narayanasamy, J.A. Selvi, S. Rajendran, *Chem. Eng. Comm.*, 195 (2008) 352.
15. P.B. Raja, M.G. Sethuraman, *Pigment & Resin Technology.* 38 (2009) 33.
16. J.C. Rocha, JACP. Gomes, E. D'Elia, *Corros. Sci.* 52 (2010) 2341.
17. A.M. Abdel-Gaber, B.A. Abd-El-Nabey, I.M. Sidahmed, A.M. El-Zayady, M. Saadawy, *Corros. Sci.* 48 (2006) 2765.
18. A.Y. El-Etre, *Corros. Sci.* 45 (2003) 2485.
19. O.K. Abiola, J.O.E. Otaigbe, O.J. Kio, *Corros. Sci.* 51 (2009) 1879.
20. O.K. Abiola, A.O. James, *Corros. Sci.* 52 (2010) 661.
21. J. Halambek, K. Berkovic, J. Vorkapic-Furac, *Corros. Sci.* 52 (2010) 3978.
22. M. Ebadi, *Pharmacodynamic Basis of Herbal Medicine*, 2nd ed., CRC Press, New York. 2007.
23. T. Hashimoto, D.J. Yun, Y. Yamada, *Phytochemistry*, 32 (1993) 713.
24. T. Hartmann, L. Witte, F. Oprach, G. Toppel, *Planta med.* 52 (1986) 390.
25. F. Ashtiana, F. Sefidkonb, *J. Med. Plants Res.* 5 (2011) 6515.
26. R.G. Parr, R.A. Donnelly, M. Levy, W.E. Palke, *J. Chem. Phys.* 68 (1978) 3801.
27. R.W. Bosch, J. Hubrecht, W.F. Bogaerts, B.C. Syrett, *Corrosion.* 57(2001) 60.
28. G. Bereket, C. Ogretir, E. Hur, *J. Mol. Struct. (THEOCHEM)*, 578 (2002) 79.
29. J. Barriga, B. Coto, B. Fernandez, *Tribol. Int.* 40 (2007) 960.
30. K.F. Khaled, *J. Solid State Electrochem.* 13 (2009) 1743.
31. Z.H. Tao, S.T. Zhang, W.H. Li, B.R. Hou, *Corros. Sci.* 51 (2009) 2588.
32. E.S. Ferreira, C. Giacomelli, F.C. Giacomelli, A. Spinelli, *Mater. Chem. Phys.* 83 (2004) 129.
33. M. Behpour, S.M. Ghoreishi, N. Mohammadi, N. Soltani, M. Salavati-Niasari, *Corros. Sci.* 52 (2010) 4046.
34. L. Larabi, Y. Harek, M. Traianel, A. Mansri, *J. Appl. Electrochem.* 34 (2004) 833.
35. M. Lebrini, M. Lagrenee, H. Vezin, M. Traisnel, F. Bentiss, *Corros. Sci.* 49(2007) 2254.
36. S. Martinez, M. Metikoš-Hukovic, *J. Appl. Electrochem.* 33 (2003) 1137.
37. M.N. El-Haddad, A.S. Fouda, *Chem. Eng. Comm.*, 200 (2013) 1366.
38. J.L. Trinstancho-Reyes, M. Sanchez-Carrillo, R. Sandoval-Jabalera, V.M. Orozco-Carmona, F. Almeraya-Calderon, J.G. Chacon-Nava, J.G. Gonzalez-Rodriguez, Martínez-Villafane, *Int. J. Electrochem. Sci.* 6 (2011) 419.
39. C.S. Hsu, F. Mansfeld, *Corrosion.* 57 (2001) 747.
40. F. Bentiss, M. Traisnel, M. Lagrenee, *Corros. Sci.* 42 (2000) 127.
41. F. Bentiss, M. Bouanis, B. Mernari, M. Traisnel, H. Vezin, M. Lagrenee, *Appl. Surf. Sci.* 253 (2007) 3696.
42. R.K. Dinnappa, S.M. Mayanna, *J. Appl. Electrochem.* 11 (1981) 111.
43. N. Patel, A. Rawat, S. Jauhari, G. Mehta, *European J. Chem.* 1 (2010) 129.
44. J.I. Bhat, V.D.P. Alva, *J. Korean. Chem. Soc.* 55 (2011) 835.
45. E.E. Oguzie, B.N. Okolue, E.E. Ebenso, G.M. Onuoha, A.I. Onuchukwu, *Mater. Chem. Phys.* 87 (2004) 394.
46. P.W. Atkins, *Physical Chemistry*, 6th Ed., Oxford University Press, 1999; p. 857.
47. S.A. Umoren, U.F. Ekanem, *Chem. Eng. Comm.*, 197 (2010) 1339.
48. K. Aramaki, N. Hackerman, *J. Electrochem. Soc.* 116 (1969) 568.
49. L. Tang, X. Li, L. Li, G. Mu, G. Liu, *Appl. Surface Sci.* 252 (2006) 6394.
50. T.P. Zhao, G.N. Mu, *Corros. sci.* 41(1999) 1937.
51. A. Döner, G. Kardas, *Corros. Sci.* 53 (2011) 4223.

52. B.G. Ateya, B.E. El-Anadouli, F.M. El-Nizamy, *Corros. Sci.* 24 (1984) 509.
53. X.H. Li, S.D. Deng, H. Fu, G.N. Mu, *Corros. Sci.* 52 (2010) 1167.
54. M.A. Amin, K.F. Khaled, S.A. Fadl-Allah, *Corros. Sci.* 52 (2010) 140.
55. G. Gao, C.H. Liang, *Electrochim. Acta.* 52 (2007) 4554.
56. K.F. Khaled, M.A. Amin, N.A. Al-Mobarak, *Appl. Electrochem.* 40 (2010) 601.
57. K.F. Khaled, S.A. Fadl-Allah, B. Hammouti, *Mater. Chem. Phys.* 117 (2009) 148.
58. G. Gece, *Corros. Sci.* 50 (2008) 2981.
59. N.O. Obi-Egbedi, I.B. Obot, *Corros. Sci.* 53 (2011) 263.
60. N.O. Eddy, B.I. Ita, *J. Mol. Model.* 17 (2011) 633.
61. L.M. Rodríguez-Valdez, A. Martínez-Villafañe, D. Glossman-Mitnik, *J. Mol. Struct. (THEOCHEM)*. 713 (2005) 65.
62. V. Cerny, *J. Optim. Theor. Appl.* 45 (1985) 41.
63. B. Delley, *J. Chem. Phys.* 92 (1990) 508.
64. R.R. Anand, R.M. Hurd, N. Hackerman, *J. Electrochem. Soc.* 112 (1965) 138.
65. E.L. Cook, N. Hackerman, *J. Phys. Chem.* 55 (1951) 549.
66. J.J. Bordeaux, N. Hackerman, *J. Phys. Chem.* 61 (1957) 1323.
67. E.E. Ebenso, N.O. Eddy, A.O. Odiongenyi, *African J. Pure. Appl. Chem.* 2 (2008) 107.
68. A.K. Singh, M.A. Quraishi, *Corros. Sci.* 52 (2010) 1529.